IEEE Access
Multidisciplinary | Rapid Review | Open Access Journal

Received October 27, 2020, accepted October 28, 2020, date of publication November 4, 2020, date of current version November 16, 2020.

Digital Object Identifier 10.1109/ACCESS.2020.3035750

79-GHz Wide-Beam Microstrip Patch Antenna and Antenna Array for Millimeter-Wave Applications

GUAN-REN SU[1], ERIC S. LI[1], TING-WEI KUO[2], HUAYAN JIN[3], (Member, IEEE), YI-CHYUN CHIANG[2], (Senior Member, IEEE), AND KUO-SHENG CHIN[2], (Senior Member, IEEE)

[1]Department of Electronic Engineering, National Taipei University of Technology, Taipei City 10608, Taiwan, R.O.C.
[2]Department of Electronic Engineering, Chang Gung University, Taoyuan City 33302, Taiwan, R.O.C.
[3]Key Laboratory of RF Circuits & System of Ministry of Education, Institute of Antennas and Microwave Technology, Hangzhou Dianzi University, Hangzhou 310018, China

Corresponding author: Kuo-Sheng Chin (kschin@mail.cgu.edu.tw)

This work was supported in part by the Ministry of Science and Technology under Grant MOST 109-2221-E-182-047, and in part by the Chang Gung University, Taiwan, R.O.C., under Grant BMRP 903.

ABSTRACT A wide-beam microstrip patch antenna and antenna array ranging from 77 to 81 GHz are presented in this study for millimeter-wave applications. A substrate-integrated-waveguide probe-fed patch was developed. For beamwidth enhancement, two I-shaped parasitic elements were placed next to the main patch to establish a three-element subarray. The current directions of the parasitic elements were opposite to that of the main patch, leading to beamwidth enhancement in the E-plane radiation pattern. The proposed I-shaped parasitic element has the advantages of coplanar structure, compact size, and easy adjustment of the induced current. An array-factor method was employed to analyze the effect of the parasitic elements on the beamwidth of the main patch. Three amplitude distributions of the subarray were compared. The distribution of $-0.1{:}1{:}-0.1$ was proved to present the most beamwidth, which can be realized easily by the proposed I-shaped parasitic elements. To achieve both wide beamwidth and high gain, a 1×8 patch antenna array with the I-shaped parasitic elements was proposed. The measured results showed that the design can offer a gain of 10.74 dBi and a wide beamwidth of 138° at 79 GHz.

INDEX TERMS Automotive radar antenna, beamwidth, parasitic element, millimeter-wave antenna, substrate integrated waveguide, wide-beam antenna.

I. INTRODUCTION

The main benefit that millimeter-wave technology has over lower RF frequencies is the wide bandwidth and small volume. In recent years, with the rapid development of application fields such as high-speed broadband wireless communication, beam scanning phase array, vehicle driver assistance, security screening, inter satellite link, imaging, and gesture recognition, the millimeter-wave band has received extensive research and application [1]–[6]. For some millimeter-wave applications, it is favorable to have an antenna with a wide beam. According to the array theory, the array pattern consists of the product of array factor and element pattern. To achieve wide-angle scanning, the element pattern of phase array should be widened to reduce scan loss. Another example is the short-range automotive radar (SRR), which requires antennas with a wide field of view up to ±65° [4].

Various 79-GHz antennas have been developed for automotive radar applications [7]–[19], but few of them exhibit a half-power beamwidth (HPBW) greater than 130°. In [7], a 1×12 slot array antenna was fabricated via low temperature co-fired ceramic (LTCC) technology. The shaped slots presented themselves in a Dolph-Chebyshev amplitude distribution, which lead to a gain of 9.6 dBi and a sidelobe level of −20 dB. A substrate-integrated-waveguide (SIW) slot-fed stacked grid antenna was introduced in [8]. This design adopted three different feed networks to create

The associate editor coordinating the review of this manuscript and approving it for publication was Chan Hwang See.

a 1 × 4 antenna array with an HPBW of 40° and a gain of 12.1 dBi. In [9], a 1 × 10 LTCC grid array antenna demonstrated an HPBW of 58° and a gain of 12.4 dBi. In [10], a planar antenna employed 1 × 8 ceramic cavities fed by slots to achieve an HPBW of 100° and a gain of 13.2 dBi. Three vertical power dividers were combined to construct a vertical feed network for a 1 × 16 patch array [11]. A gain of 13 dBi was observed. In [12], a 1 × 8 grid antenna developed through multi-layer PCB technology produced an HPBW of 62° and a gain of 13.52 dBi. A compact comb-line array antenna was proposed for beamwidth enhancement [13]. A wide HPBW of 124° and a gain of 12.36 dBi were achieved. In [15], dual-polarized antenna arrays using inclined 45° patches were presented for automotive radars. In [17], a transition structure from a microstrip line to a ridge gap waveguide (GWG) was proposed for a slot antenna array with a magnetic-coupling ridge GWG feed network operating at 77 and 79 GHz. A Luneburg lens and seventeen SIW-fed log periodic dipole arrays were integrated into a lens antenna [18]. The measured results demonstrated the capability of a wide scanning angle of ±85° in an azimuth plane. In [19], a cavity-backed bow-tie microstrip antenna was introduced to offer a gain of 7.9 dBi and beamwidths of 84° in E-plane and 48° in H-plane.

There have been many techniques proposed to increase antenna beamwidths at low operating frequencies [20]–[26]. A slot antenna from [20] employed a pair of tapered slots and patches to guide its surface current. The E-plane and H-plane beamwidths of this antenna can be extend to surpass 117°. A dual-polarized antenna presented in [21] consisted of four differentially-fed patches, four short-circuited vias, and a square metallic cavity. The measured beamwidth in E-plane was greater than 116°. The design developed in [22] explored a multi-resonant patch antenna fed by a coupling slot. The beamwidth of this structure could reach 125°. An SIW-based slot antenna was proposed in [23]. By integrating the structures of magnetic and electric dipoles, a wide beamwidth of 140° was observed in both E- and H-planes. A conformal magneto-electric dipole with wide H-plane pattern for base-station applications was presented in [24]. In [25], a circularly-polarized magneto-electric dipole with meta-columns loading can achieve wide beamwidth of greater than 108° in principle planes. A patch antenna from [26] adopts a double-layer design. A main patch was located at the bottom of the structure, whereas a parasitic ring was placed on the top. A field pattern similar to the one generated by a magnetic dipole antenna was created through this parasitic ring, and superimposed to the radiation pattern of the main patch to achieve a beamwidth of 140°. The antenna arrays in [27], [28] consist of patches and parasitic elements. Parasitic elements were used to reduce the gain of the main patch to increase the beamwidth of the antenna array. Although the widest antenna beamwidth from the above studies could exceed 130°, its operating frequency was far below 79 GHz.

This work presents a wide-beam microstrip patch antenna and a 1 × 8 patch antenna array operating over the frequency range from 77 to 81 GHz. The following innovative techniques have been used in this design, which are helpful to improve the performance of conventional patch antennas:

(i) SIW probe-fed patch antenna: the SIW feed line and probe-fed structure were combined to minimize the insertion loss and to increase the beamwidth of patch antennas;

(ii) Three-element subarray: two parasitic elements were added laterally to the main patch to establish a three-element subarray. The current directions of the parasitic elements were opposite to that of the main patch, leading to beamwidth enhancement;

(iii) I-shaped parasitic element: the proposed I-shaped parasitic element has the advantages of coplanar structure, compact size, and easy adjustment of the induced current;

(iv) Analysis method: an array-factor method was proposed to analyze the effect of the parasitic elements on the beamwidth of the main patch. The distribution of −0.1:1:−0.1 was proved to present the most beamwidth, which can be realized easily by the proposed I-shaped parasitic elements;

(v) Beamwidth and gain enhancement technique: a 1 × 8 patch antenna array with the I-shaped parasitic elements was proposed to achieve both wide beamwidth and high gain. The measured results showed that the design can offer a gain of 10.74 dBi and a wide beamwidth of 138° at 79 GHz.

The rest of this paper is organized as follows: The design of an SIW probe-fed patch antenna is described in Section II. The main patch is laterally loaded with two I-shaped parasitic elements for bandwidth enhancement as disclosed in Section III. In Section IV, a 1 × 8 patch antenna array is introduced to provide additional gain besides wide beamwidth. At last, the paper is concluded in Section V.

II. DESIGN OF SIW PROBE-FED PATCH ANTENNA

Patch antennas are one of the most popular designs for planar antennas. However, conventional microstrip edge-fed patch antennas normally exhibit an HPBW around 80° [29], which is insufficient to cover the desired wide field of view 130° (or ±65°) demanded by SRR applications [4]. The beamwidth of a patch antenna can be enhanced if it is fed by a probe [30]. In addition, the insertion loss of microstrip feed lines becomes considerable in millimeter-wave band. The SIW feed line can be chosen as an alternative to minimize the insertion loss [31].

Fig. 1 shows the configuration of an SIW probe-fed patch antenna. The structure consists of two substrates and three metallic layers. The SIW portion is constructed in Sub 2 with one end terminated by a metallic via wall. A circular aperture is created on the top surface of the SIW and is located at $0.33\lambda_g$ from the termination, where λ_g is the guided wavelength. The feed probe penetrates through the two substrates and the aperture to support a vertical excitation current. One end of the probe is connected to the bottom surface of the SIW, and the other end is connected to the patch antenna. The radiation generated by the feed probe is superposed to the pattern of the patch antenna to increase the beamwidth of the latter. The laminate Roger 4450F with a dielectric constant

of 3.52 and a thickness of 0.203 mm was selected for Sub 1, while the laminate Roger 4350B with a dielectric constant of 3.66 and a thickness of 0.254 mm was chosen for Sub 2.

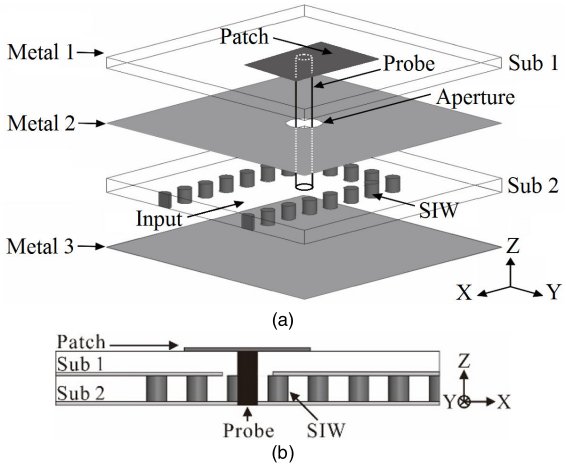

FIGURE 1. Configuration of the SIW probe-fed patch antenna: (a) 3D view. (b) Side view.

The impedance of the feed probe is determined by the dielectric constant and thickness of the substrate, the diameters of the aperture and via hole, and the position of the aperture. When the dielectric constant and thickness of the substrate and the diameter of via holes are fixed, the location and size of the aperture would affect the impedance matching of the feed network. To analyze the feed structure separately, the two-port network of the SIW probe-fed structure with $p = 0.4$ mm and $d = 0.2$ mm is established and presented in Fig. 2, in which Sub 1 and Metal 1 are removed. The diameter of the feed probe is 0.2 mm. The full-wave EM software HFSS was employed to conduct the required simulations for this work.

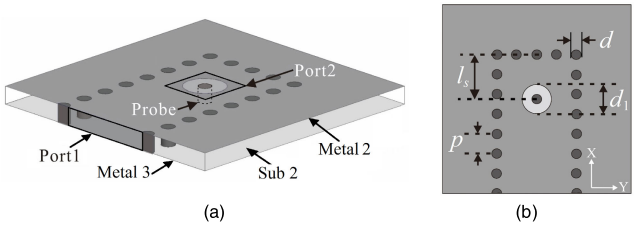

FIGURE 2. Two-port network of the SIW probe-fed structure after removing Sub 1 and the patch antenna: (a) 3D view. (b) Top view.

Fig. 3 shows the simulated S-parameter responses of the two-port network. The slot position l_s and diameter d_1 will affect the return loss and resonant frequency. However, increasing the values of l_s and d_1 has an opposite effect on the S-parameter responses. Based on optimization, the values of l_s and d_1 are selected to be 0.9 mm and 0.6 mm, respectively. According to the results shown in Fig. 3, the proposed SIW probe-fed network has a low insertion loss of less than 1 dB and a high return loss of more than 14 dB within the frequency range of 77−81 GHz, which confirms good impedance matching performance.

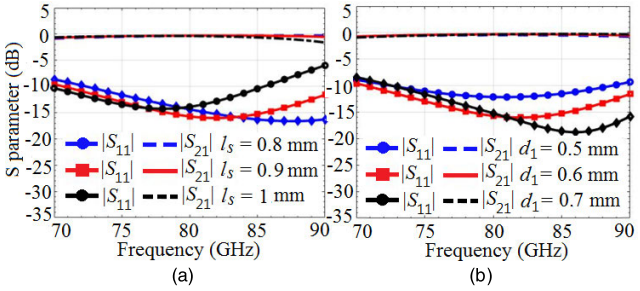

FIGURE 3. Simulated S-parameter responses of the SIW probe-fed structure in Fig. 2 subject to the changes in: (a) the aperture position l_s ($d_1 = 0.6$ mm) and (b) the aperture diameter d_1 ($l_s = 0.9$ mm).

Fig. 4 shows a patch antenna fed by the proposed SIW probe-fed network. The simulated $|S_{11}|$ responses of the SIW probe-fed patch antenna subject to the changes in the patch length L_1 and the probe position y_0 are illustrated in Fig. 5. The parameter L_1 is the resonance length corresponding to the operating frequency. Based on the results displayed in Fig. 5(a), the value of 0.82 mm is suitable for the operations at 79 GHz. The value of W_1 is chosen to be one and a half times the length of L_1. The position y_0 affects the return loss of the patch antenna. The antenna would achieve its optimum matching performance if y_0 is chosen as 0.16 mm. According to the curves observed in Fig. 5, the −10-dB impedance bandwidth of the SIW probe-fed patch antenna ranges from 75.85 GHz to 82.21 GHz, which amounts to 8.04%.

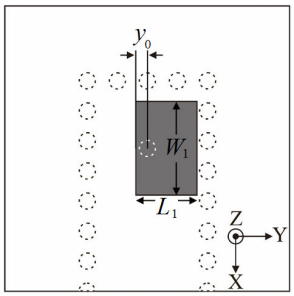

FIGURE 4. Design parameters of the SIW probe-fed patch antenna.

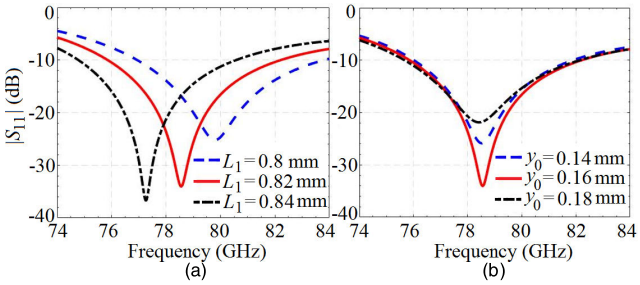

FIGURE 5. Simulated $|S_{11}|$ responses of the SIW probe-fed patch antenna subject to the changes in: (a) the patch length L_1 and (b) the probe position y_0.

Fig. 6 shows the simulated radiation patterns of the patch antenna at 79 GHz, of which its HPBW is 91°. The maximum gain is 6.7 dBi. The beamwidth of the E-plane co-polarized

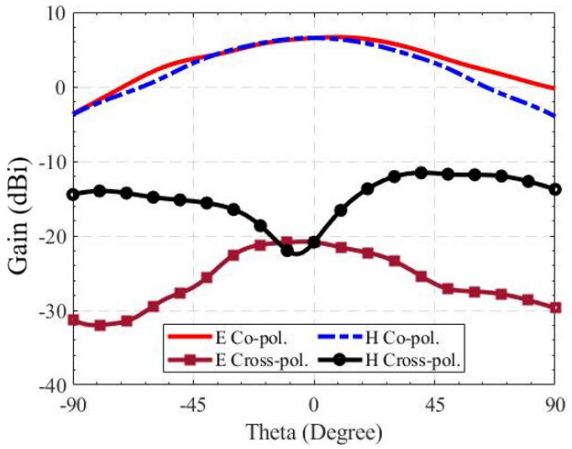

FIGURE 6. Simulated radiation patterns of the SIW probe-fed patch antenna at 79 GHz.

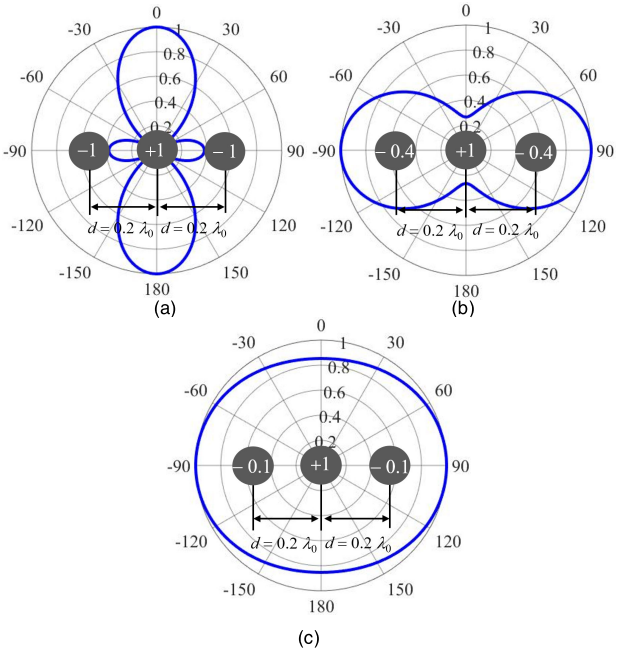

FIGURE 7. Normalized radiation patterns of the array factor of a three-element subarray subject to different ratios of current amplitudes: (a) Case 1, −1:1:−1. (b) Case 2, −0.4:1:−0.4. (c) Case 3, −0.1:1:−0.1.

pattern is slightly wider than that of the H-plane pattern. At angles other than 0°, the level of the H-plane cross-polarized pattern is more severe than the level of the E-plane pattern, which is a unique feature of patch antennas with single-ended feed. The SIW probe-fed method can widen the beamwidth of the patch antenna, but its effect is limited, and the beamwidth does not meet the design goal.

III. DESIGN OF WIDE-BEAM PATCH ANTENNA WITH I-SHAPED PARASITIC ELEMENTS

A. THREE-ELEMENT SUBARRAY

According to the array theory [29], the complete pattern of an array antenna can be obtained from the element pattern of a single element antenna of the array multiplied by the pattern

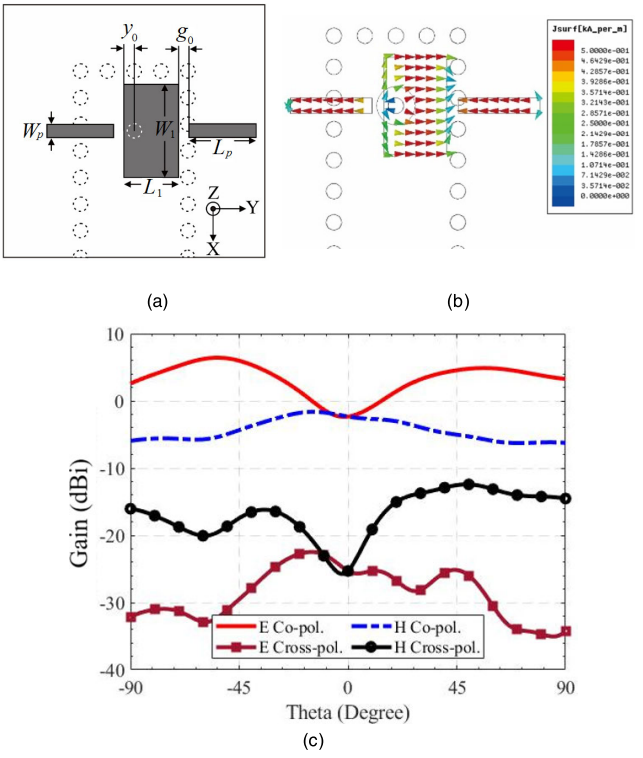

FIGURE 8. SIW probe-fed patch antenna loaded with two parasitic strips: (a) Top view. (b) Surface current distributions at 79 GHz. (c) Radiation patterns at 79 GHz. (L_p = 1 mm, W_p = 0.2 mm, and g_0 = 0.15 mm).

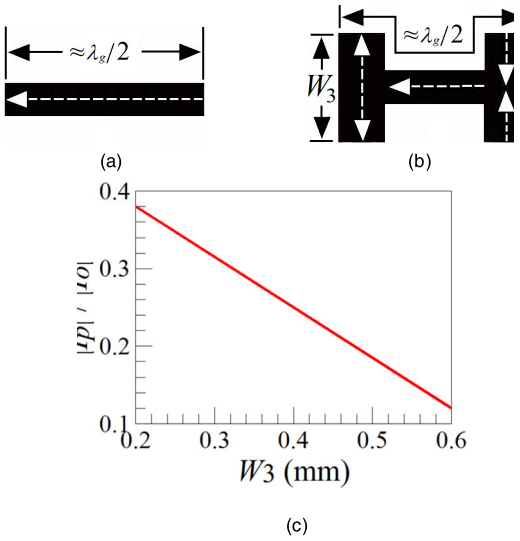

FIGURE 9. Current distributions on (a) a uniform strip and (b) an I-shaped parasitic element. (c) Current ratio $|I_P/I_O|$ subject to the width W_3 of the I-shaped parasitic element.

of a normalized array factor. For beamwidth enhancement, parasitic elements are introduced to expand the radiation pattern of the probe-fed patch antenna. Two parasitic elements are added laterally to the main patch to establish a three-element subarray.

The influence of the parasitic elements on the radiation pattern of the main patch can be analyzed through the array

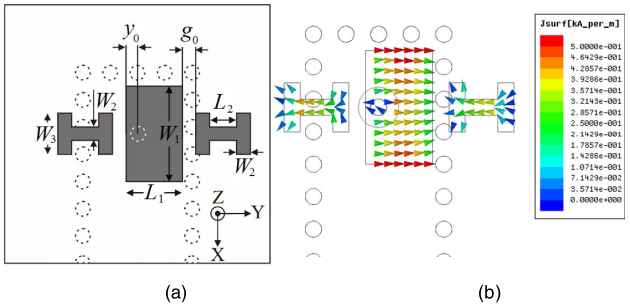

FIGURE 10. SIW probe-fed patch antenna loaded with two I-shaped parasitic elements: (a) Top view. (b) Surface current distributions at 79 GHz.

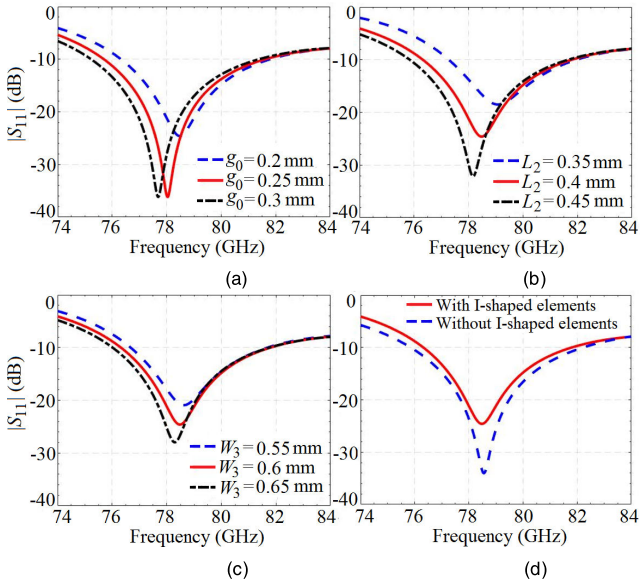

FIGURE 11. Simulated $|S_{11}|$ responses of the patch antenna loaded with I-shaped parasitic elements subject to the changes in: (a) g_0, (b) L_2, and (c) W_3. (d) Simulated $|S_{11}|$ responses of the patch antenna with and without the I-shaped parasitic elements.

TABLE 1. Values of the Design Parameters for the Proposed Patch Antenna With the I-Shaped Parasitic Elements (in mm).

p	l_s	L_1	L_2	g_0	y_0
0.4	0.9	0.82	0.4	0.2	0.16
d	d_1	W_1	W_2	W_3	
0.2	0.6	1.4	0.2	0.6	

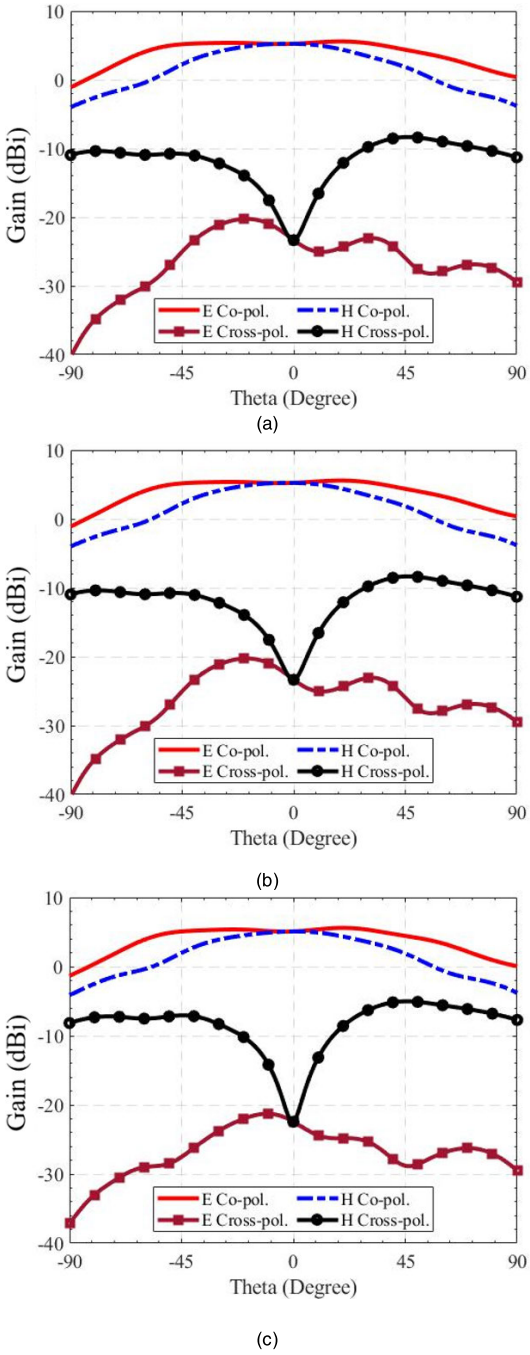

FIGURE 12. Simulated radiation patterns of the SIW probe-fed patch antenna with the I-shaped parasitic elements at: (a) 77 GHz, (b) 79 GHz, and (c) 81 GHz.

factor. The key design parameters are the spacing between the elements and the ratios of the current amplitudes of the elements. The spacing would affect the amount of the energy coupled from the main patch to the parasitic elements and, therefore, the superposition mechanism of the radiation patterns. The center-to-center spacing of the elements is chosen as $0.2\lambda_0$, where λ_0 is the wavelength in free space, which is enough to prevent the parasitic elements short to the main patch. For simplicity, Fig. 7 shows the normalized radiation patterns of an array factor associated with three isotropic point sources. Three amplitude distributions of the three-element subarray were examined to compare their influence on the array factor: −1:1:−1 (Case 1), −0.4:1:−0.4 (Case 2), and −0.1:1:−0.1 (Case 3). The negative amplitude indicates that the element-to-element phase shift is 180. As the current of the parasitic element increases, the radiation null and beam focusing will happen in the direction of broadside, resulting in the reduction of beamwidth. Fig. 7(c) shows a wide pattern generated by the amplitude distribution of Case 3 as opposed to the nulls produced by those from Cases 1 and 2.

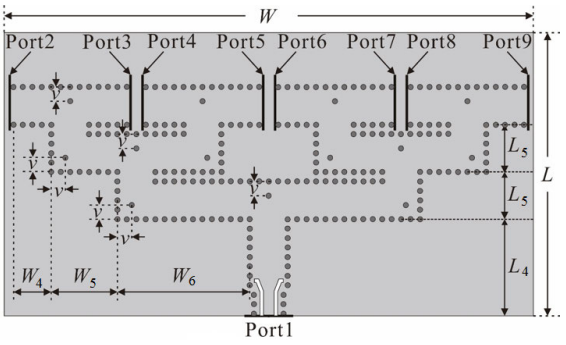

FIGURE 13. Structure of the proposed eight-way SIW feed network.

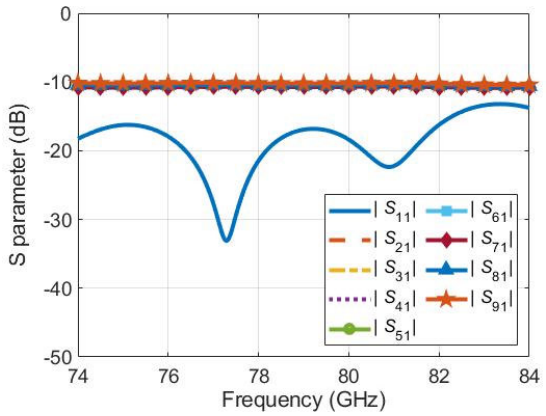

FIGURE 14. Simulated *S*-parameter responses of the eight-way SIW feed network.

TABLE 2. Performance of the Proposed Patch Antenna With the I-Shaped Parasitic Elements.

−10-dB Bandwidth	76.3–81.7 GHz (6.8%)		
	77 GHz	79 GHz	81 GHz
Gain (dBi)	5.25	5.21	5.07
E-plane HPBW	138°	138°	135°
H-plane HPBW	83°	85°	85°

B. DESIGN OF PARASITIC ELEMENTS

To widen the E-plane beamwidth, the parasitic elements should affect the E-plane pattern of the main patch, but need to avoid affecting the H-plane pattern to maintain the gain. The first candidate for the parasitic elements is a uniform strip. Fig. 8(a) reveals the initial design of the three-element subarray, in which the two parasitic strips were placed next to the E-plane sides of the main patch with a length of $\approx 0.5\lambda_g$ and a width of 0.2 mm. The spacing of the three-element subarray is $0.26\lambda_0$. The direction of induced strip currents is expected to be opposite to that of the current on the main patch, which would reduce the antenna gain in return for an increase in beamwidth. The prediction is confirmed by the current distributions of the subarray at 79 GHz, as shown in Fig. 8(b). By resorting to the function of Field Overlays from HFSS, the ratios of the current amplitudes on the three-element subarray were given by −0.37:1:−0.38, which is close to the amplitude distribution specified by Case 2. Fig. 8(c) shows the simulated radiation patterns of the three-element subarray at 79 GHz. The presence of the parasitic elements indeed expands the patch antenna beam. However, excessive currents on the parasitic strips generate a radiation null at the angle of 0°, which effectively narrows down the HPBW. This result is consistent with the pattern of Case 2 shown in Fig. 7(b).

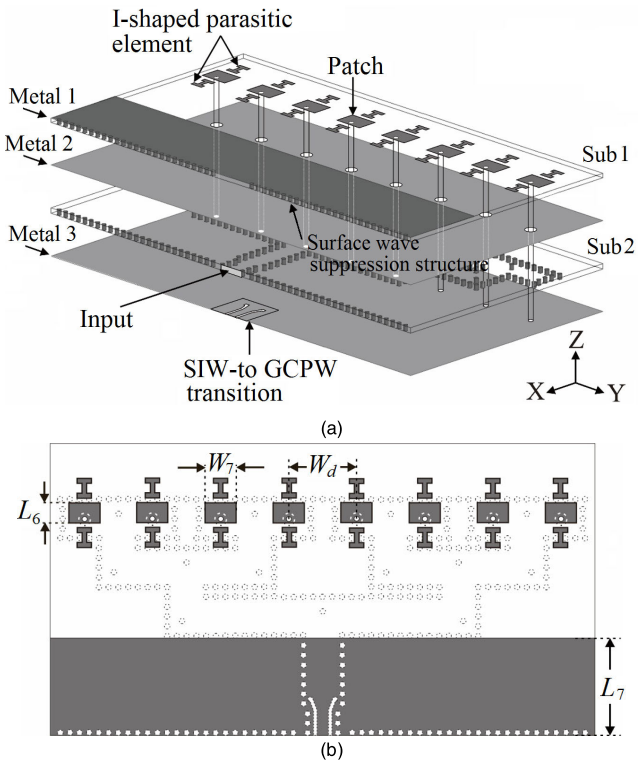

FIGURE 15. Configuration of the proposed 1 × 8 patch antenna array: (a) 3D view and (b) Top view.

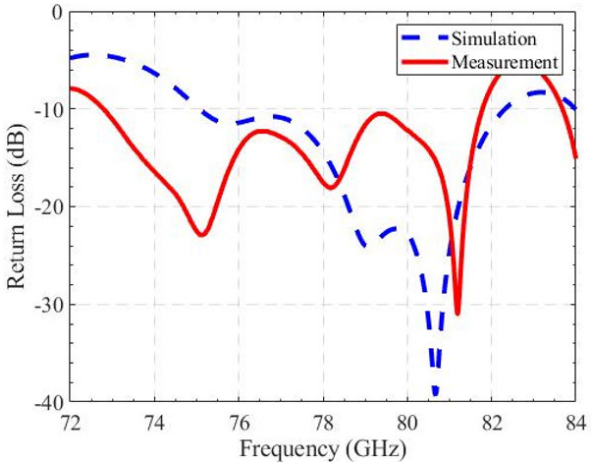

FIGURE 16. Simulated and measured $|S_{11}|$ responses of the proposed 1 × 8 patch antenna array.

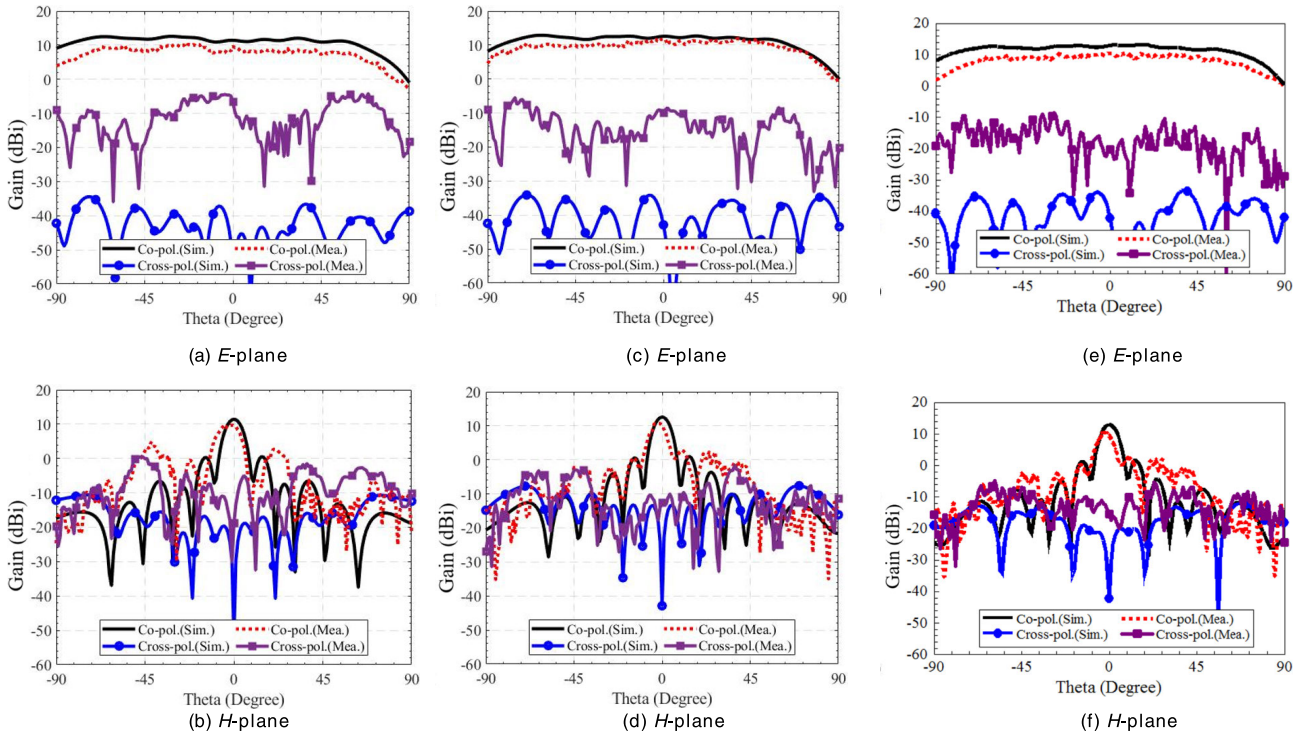

FIGURE 17. Simulated and measured radiation patterns of the proposed 1 × 8 patch antenna array. At 77 GHz: (a) *E*-plane and (b) *H*-plane. At 79 GHz: (c) *E*-plane and (d) *H*-plane. At 81 GHz: (e) *E*-plane and (f) *H*-plane.

To solve the problem caused by the excessive currents, an I-shaped parasitic element with the same resonance length is proposed to replace the uniform strip. Since the vertical sections at both ends of the I shape will force the current to flow in the opposite direction, it can be used to adjust the current amplitude of the parasitic element. Note that when changing the size of the parasitic element to adjust current amplitude, the equivalent electrical length of the parasitic element still needs to maintain a resonance length of $0.5\lambda_g$ to ensure that the current phase is reversed.

Figs. 9(a) and 9(b) compare the current distributions of the uniform strip and the I-shaped parasitic element. The currents on both ends of the I-shaped element are out of phase to each other, thus reducing the total current amplitude. Compared with the uniform strip, the vertical sections of the I-shaped parasitic element provide additional design freedom, which is useful for adjusting the amplitude of the induced current to solve the problem of the radiation null. Fig. 9(c) shows the width W_3 of the I-shaped parasitic element required for the current ratio $|I_p/I_o|$ adjustment, where I_p and I_o are the current of the parasitic element and the main patch, respectively.

Fig. 10(a) shows two proposed I-shaped parasitic elements to replace the uniform strips. The desired current distribution is created and displayed in Fig. 10(b). Figs. 11(a)−11(c) disclose the simulated $|S_{11}|$ responses of the patch antenna loaded with two I-shaped parasitic elements subject to the changes in the values of the design parameters, g_0, L_2, and W_3, respectively. The two parameters g_0 and L_2 demonstrate a more significant influence on the resonant frequency as well as the return loss than the parameter W_3. According to the simulation results, the values of $g_0 = 0.2$ mm, $L_2 = 0.4$ mm, and $W_3 = 0.6$ mm would lead to the best performance in terms of impedance matching. The ratios of the current amplitudes calculated by HFSS are −0.14:1:−0.12, which is close to the current distribution of the array factor specified in Case 3.

C. SIMULATION RESULTS OF PATCH WITH PARASITIC ELEMENTS

Fig. 11(d) shows the simulated $|S_{11}|$ responses of the probe-fed patch antenna with and without the I-shaped parasitic elements. The −10-dB return-loss bandwidth of the one with the parasitic elements ranges from 76.3 GHz to 81.7 GHz, which is equivalent to 6.8% and is slightly less than the bandwidth of the one without the parasitic elements.

Figs. 12(a)−12(c) show the simulated radiation patterns of the proposed antenna at 77 GHz, 79 GHz, and 81 GHz, respectively. Because the direction of the currents on parasitic elements towards the *E*-plane, the *H*-plane current of the main patch will not be disturbed. Therefore, the beamwidth of the *E*-plane co-polarized pattern is much wider than the beamwidth of the *H*-plane pattern. At 79 GHz, a gain of 5.21 dBi is achieved. A wide HPBW of 138° is also observed, which is 47° greater than that of the antenna without the I-shaped parasitic elements. The HPBW in the *H*-plane is only slightly affected by the presence of the I-shaped parasitic elements. Table 1 lists the values of the design parameters for the proposed wide-beam patch antenna.

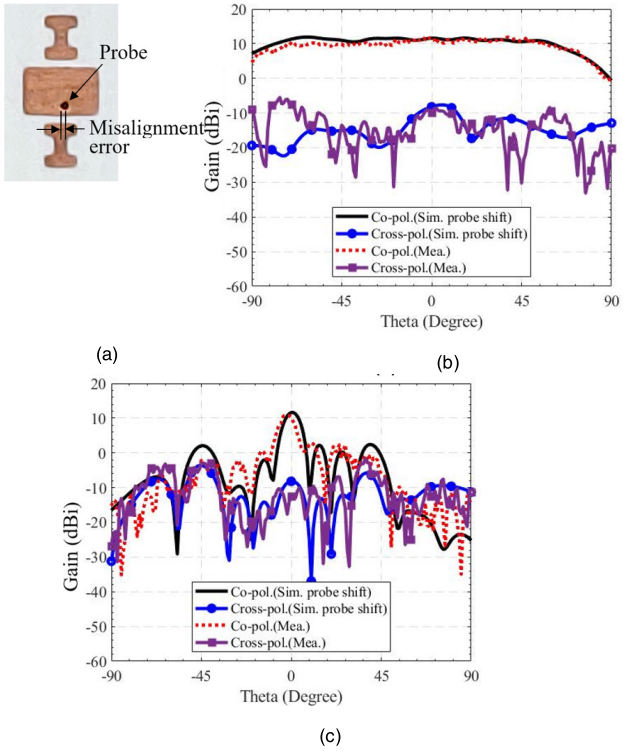

FIGURE 18. (a) Zoom-in view of the patch loaded by two I-shaped parasitic elements. Simulated radiation patterns in the (b) *E*-plane and (c) *H*-plane of the 1 × 8 patch antenna array at 79 GHz with its probes misaligned by 0.1 mm.

The comprehensive performance of the antenna at the three frequencies is provided in Table 2.

Note that the proposed parasitic elements are not limited to being arranged only along the E-plane direction of the antenna. This work chose to enhance the E-plane beamwidth of the antenna because the horizontally-polarized automotive radar antenna was selected as a design example.

IV. WIDE-BEAM HIGH-GAIN 1 × 8 PATCH ANTENNA ARRAY WITH I-SHAPED PARASITIC ELEMENTS

A. DESIGN PROCEDURE

For convenience of applications, the basic steps for the wide-beam patch antenna design are summarized as follows.

Step 1) Determine the size of SIW probe-fed structure based on the operating frequency and two-port network analysis.

Step 2) Combine the patch antenna and SIW probe-fed structure, and adjust the circuit size to achieve superior impedance matching.

Step 3) Adjust the spacing and size of the I-shaped parasitic elements according to the required current ratio.

Step 4) Design the array feed network according to the required number of elements and the array spacing.

Step 5) Complete the antenna array design.

B. 1 × 8 PATCH ANTENNA ARRAY

To feature both wide beamwidth and high gain, a 1 × 8 patch antenna array with I-shaped parasitic elements is proposed.

TABLE 3. Values of the Design Parameters for the Proposed 1 × 8 Patch Antenna Array (in mm).

L	W	L_4	L_5
12	22.4	3.1	2
W_4	W_5	W_6	V
1.6	2.8	5.6	0.6
L_6	L_7	W_7	W_d
0.82	4	1.3	2.8

TABLE 4. Comparison on the Performances of the 1 × 8 Patch Antenna Array With and Without the I-Shaped Parasitic Elements.

With/Without I-Shaped Elements	With						Without		
	Simulated			Measured			Measured		
−10-dB Bandwidth (GHz)	75–82.3 (9.28%)			72.79–81.78 (11.63%)			73.51–81.84 (10.72%)		
	77	79	81	77	79	81	77	79	81
Gain (dBi)	11.42	12.57	13	9.69	10.74	10.58	11.38	12.47	12.1
E-plane HPBW(°)	145	144	140	137	138	130	96	93	90
H-plane HPBW(°)	8	8	8	8	8	8	8	8	8

Generally, the bandwidth of series-fed array is more limited than that of the parallel-fed array. Moreover, series-fed array may introduce frequency-dependent progressive phase increments to the radiating elements, resulting in the radiation pattern changing with frequency. Therefore, a parallel feed is proposed to keep the radiation patterns constant across the whole bandwidth.

Fig. 13 shows the structure of the corresponding eight-way SIW feed network. The via holes placed in the centers and corners of the T-junction power dividers serve the purposes of power equalization and impedance matching. Note that the eight wave ports (Port 2−Port 9) marked in SIW feed network are only used for the preliminary S-parameter analysis, which do not include the feed probes and apertures. Fig. 14 shows the simulated S-parameter responses of the SIW feed network. The insertion loss of each transmission path is less than −1 dB and $|S_{11}|$ is lower than −15 dB across the frequency range of 77−81 GHz.

The SIW feed network is integrated with the eight patches accompanied by the I-shaped parasitic elements to complete the proposed design. The substrate adopted for the single probe-fed patch antenna in Section II also serves for the array antenna. More investigations on PCB laminates for automotive radar antennas under various environmental conditions are disclosed in [32]. The array pitch of the patch antennas is $0.73\lambda_0$.

Fig. 15 shows the configuration of the proposed 1 × 8 patch antenna array. The patch antennas and the SIW feed network are fabricated in Sub 1 and Sub 2, respectively.

TABLE 5. Comparison on the Performance of the Proposed Antenna Array and Previously Reported 79-GHz Antennas.

Ref.	Frequency (GHz)	Antenna type	Polarization	Element number	HPBW *E*-plane/*H*-plane	Bandwidth ($\|S_{11}\|$<−10 dB)	Peak gain (dBi)	Size (mm^3)
[7]	79	Laminated waveguide array antenna with shaped slots	Horizontal	1×12	NP/10°	3.03%	9.6	NP
[8]	79	SIW slot-fed stacked double grid antenna	Vertical	1×4	12°/40°	11.3%	12.1	16.6×10.9×0.1
[9]	79	Grid array antenna	Vertical	1×10	16°/58°	15.2%	12.4	NP
[10]	79	Slot array with ceramic-filled cavity resonators	Vertical	1×8	13°/100°	8.2%	13.2	NP
[11]	79	Patch array with LWG-based vertical parallel feed	Vertical	1×16	7°/NP	6.3% ($\|S_{11}\|$<−15 dB)	13	28.3×1.2×1.62
[12]	79	Grid array constructed by multilayer PCB technology	Vertical	1×8	12°/62°	16.8%	13.52	NP
[13]	79	Comb-line array	Horizontal	1×16	124°/10.5° (Simulation)	12.5%*	12.36	NP
[14]	79	Slotted SIW antenna	Linear	4×4	33°/31°#	10.7%	11	14×10.9×0.08
[15]	78	Dual-polarized square patch array	Dual polarization	1×10	10° (Elevation) 90° (Azimuth)	>7.7%	10	30×16×0.13
[17]	77/79	Slot array with ridge GWG feeding network	Linear	8×8	16°/16°#	6%	18.3	NP
[19]	79	Cavity backed bow-tie microstrip antenna	Linear	1×2	48°/82°	9.25%	7.9	NP
This work	**79**	**Patches loaded with I-shaped parasitic elements**	**Horizontal**	**1×8**	**138°/8°**	**11.63%**	**10.74**	**23×12×0.46**

NP: Not provided. *: The 3-dB gain bandwidth is also considered. #: Calculated from the graph of the referenced paper.

An SIW-to-GCPW transition is introduced to benefit measurements. Note that a surface wave suppression structure consisting of a rectangular ground plane on Sub 1 and via wall in Sub 1 is added to reduce the surface wave effect [33]. Table 3 lists the detailed dimensions of this array antenna.

C. SIMULATION AND MEASUREMENT RESULTS

Fig. 16 shows the simulated and measured $|S_{11}|$ responses of the proposed 1 × 8 patch antenna array. The measured −10-dB impedance bandwidth ranges from 72.79 to 81.78 GHz, which amounts to 11.63%. The result is in good agreement with the simulated bandwidth ranging from 75−82.3 GHz, which is equivalent to 9.28%. The center frequency is slightly shifted to low frequency, which is due to the fact that the actual dielectric constants of RO4350B and RO4450F at 79 GHz are slightly higher than the values substituted in the simulation.

Figs. 17 display the *E*-plane and *H*-plane radiation patterns of the proposed 1 × 8 patch antenna array at 77 GHz, 79 GHz, and 81 GHz. As indicated in Figs. 17(c) and 17(d), the simulated and measured gains at 79 GHz are 12.57 dBi and 10.74 dBi, respectively. The simulated and measured HPBWs in the *E*-plane are 144° and 138°, respectively, in contrast to the value of 8° in the *H*-plane. No significant changes in the antenna patterns are observed at these three frequencies. The simulated cross-polarization level is more than 40 dB below the co-polarization level in the *E*-plane. However, only 20-dB difference is noticed between the measured cross- and co-polarization levels in the vicinity of the boresight direction. The increase in cross-polarization level and the decrease in gain are likely caused by the fabrication and assembly errors, in which the feed probes were misaligned by 0.1 mm leading to undesired excitation currents on the patches.

Fig. 18(a) shows the zoom-in view of a patch loaded by two I-shaped parasitic elements. The picture clearly shows the misalignment of the feed probe. This speculation can be verified by the simulated radiation patterns of the 1 × 8 patch antenna array with the feed probes misaligned by 0.1 mm. As indicated in Figs. 18(b) and 18(c), the simulated results are quite consistent with the measured results, which confirm that the misalignment of the feed probes would severely degrade the antenna gain and the cross polarization level.

Table 4 summaries the simulated and measured performance of the proposed 1 × 8 patch antenna array. The comparison on the measured performance of the 1 × 8 patch antenna array with and without the I-shaped parasitic elements is provided in Table 4 along with the simulated performance of the proposed antenna array. The table indicates that the presence of the I-shaped parasitic elements enhances the *E*-plane beamwidth of the patch antenna array. The photo of the final assembled 1 × 8 patch antenna array with the I-shaped parasitic elements is shown in Fig. 19. Table 5 compares the performance of the proposed antenna array

and other published 79-GHz antennas. The proposed antenna array outperforms other designs on its E-plane beamwidth.

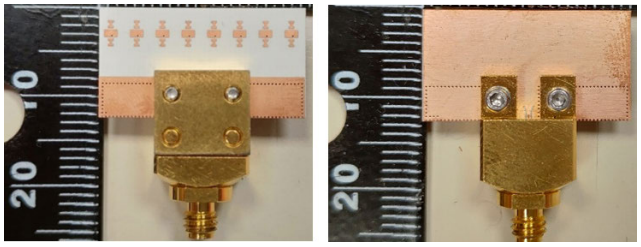

(a) (b)

FIGURE 19. Final assembled antenna array: (a) Top view. (b) Bottom view.

V. CONCLUSION

This study presents a wide-beam patch antenna for millimeter-wave applications ranging from 77 to 81 GHz. A SIW probe-fed patch was developed. For beamwidth enhancement, two parasitic elements were added to the main patch to enhance the beamwidth. An array-factor method was used to analyze the influence of parasitic elements on the main patch. The ratio of the current amplitudes of the three-element subarray was investigated. The distribution of $-0.1{:}1{:}-0.1$ was proved to present the most beamwidth. According to the analysis result, two I-shaped parasitic elements placed next to the E-plane sides of the main patch achieved this goal. The proposed I-shaped parasitic element provides additional design freedom, which is useful for the amplitude adjustment of the induced current. A 1×8 patch antenna array with the proposed I-shaped parasitic elements was assembled for both wide beamwidth and gain enhancement. An HPBW of 138° and a gain of 10.74 dBi were observed at 79 GHz.

REFERENCES

[1] S. Ghosh and D. Sen, "An inclusive survey on array antenna design for millimeter-wave communications," *IEEE Access*, vol. 7, pp. 83137–83161, 2019.
[2] S. Wang, Q. Zhu, and S. Xu, "Design of a compact millimeter-wave microstrip antenna with wide bandwidth and broad beamwidth," *Int. J. Infr. Millim. Waves*, vol. 28, no. 7, pp. 513–519, May 2007.
[3] S.-T. Ko and J.-H. Lee, "Aperture coupled metamaterial patch antenna with broad E-plane beamwidth for millimeter wave application," in *Proc. IEEE Antennas Propag. Soc. Int. Symp. (APSURSI)*, Jul. 2013, pp. 1796–1797.
[4] J. Wenger, "Short range radar–being on the market," in *Proc. Eur. Radar Conf.*, Munich, Germany, Oct. 2007, pp. 255–258.
[5] B. Mamandipoor, G. Malysa, A. Arbabian, U. Madhow, and K. Noujeim, "60 GHz synthetic aperture radar for short-range imaging: Theory and experiments," in *Proc. 48th Asilomar Conf. Signals, Syst. Comput.*, Pacific Grove, CA, USA, vol. 558, Nov. 2014, p. 553.
[6] M. Kucharski, A. Ergintav, W. A. Ahmad, M. Krstic, H. J. Ng, and D. Kissinger, "A scalable 79-GHz radar platform based on single-channel transceivers," *IEEE Trans. Microw. Theory Techn.*, vol. 67, no. 9, pp. 3882–3896, Sep. 2019.
[7] F. Bauer and W. Menzel, "A 79-GHz resonant laminated waveguide slotted array antenna using novel shaped slots in LTCC," *IEEE Antennas Wireless Propag. Lett.*, vol. 12, pp. 296–299, Feb. 2013.
[8] O. Khan, J. Meyer, K. Baur, and C. Waldschmidt, "Hybrid thin film antenna for automotive radar at 79 GHz," *IEEE Trans. Antennas Propag.*, vol. 65, no. 10, pp. 5076–5085, Oct. 2017.
[9] F. Bauer, X. Wang, W. Menzel, and A. Stelzer, "A 79-GHz radar sensor in LTCC technology using grid array antennas," *IEEE Trans. Microw. Theory Techn.*, vol. 61, no. 6, pp. 2514–2521, Jun. 2013.
[10] F. Bauer and W. Menzel, "A 79-GHz planar antenna array using ceramic-filled cavity resonators in LTCC," *IEEE Antennas Wireless Propag. Lett.*, vol. 12, pp. 910–913, Jul. 2013.
[11] X. Wang and A. Stelzer, "A 79-GHz LTCC patch array antenna using a laminated waveguide-based vertical parallel feed," *IEEE Antennas Wireless Propag. Lett.*, vol. 12, pp. 987–990, Aug. 2013.
[12] M. Mosalanejad, I. Ocket, C. Soens, and G. A. E. Vandenbosch, "Multilayer compact grid antenna array for 79 GHz automotive radar applications," *IEEE Antennas Wireless Propag. Lett.*, vol. 17, no. 9, pp. 1677–1681, Sep. 2018.
[13] M. Mosalanejad, I. Ocket, C. Soens, and G. A. E. Vandenbosch, "Wide-band compact comb-line antenna array for 79 GHz automotive radar applications," *IEEE Antennas Wireless Propag. Lett.*, vol. 17, no. 9, pp. 1580–1583, Sep. 2018.
[14] S. Cheng, H. Yousef, and H. Kratz, "79 GHz slot antennas based on substrate integrated waveguides (SIW) in a flexible printed circuit board," *IEEE Trans. Antennas Propag.*, vol. 57, no. 1, pp. 64–71, Jan. 2009.
[15] G. F. Hamberger, S. Spath, U. Siart, and T. F. Eibert, "A mixed circular/linear dual-polarized phased array concept for automotive radar–planar antenna designs and system evaluation at 78 GHz," *IEEE Trans. Antennas Propag.*, vol. 67, no. 3, pp. 1562–1572, Mar. 2019.
[16] H. Tian, C. Liu, and X. Gu, "Proximity-coupled feed patch antenna array for 79 GHz automotive radar," *J. Eng.*, vol. 2019, no. 19, pp. 6244–6246, Oct. 2019.
[17] Y. Shi, W. Feng, H. Wang, W. Che, Q. Xue, J. Wang, J. Zhang, X. Qian, M. Zhou, and B. Cao, "Novel W-band LTCC transition from microstrip line to ridge gap waveguide and its application in 77/79 GHz antenna array," *IEEE Trans. Antennas Propag.*, vol. 67, no. 2, pp. 915–924, Feb. 2019.
[18] M. K. Saleem, H. Vettikaladi, M. A. S. Alkanhal, and M. Himdi, "Lens antenna for wide angle beam scanning at 79 GHz for automotive short range radar applications," *IEEE Trans. Antennas Propag.*, vol. 65, no. 4, pp. 2041–2046, Apr. 2017.
[19] M. Mosalanejad, I. Ocket, C. Soens, and G. A. E. Vandenbosch, "Multi-layer PCB bow-tie antenna array for 77-81 GHz radar applications," *IEEE Trans. Antennas Propag.*, vol. 68, no. 3, pp. 2379–2386, Mar. 2020.
[20] F. Zhang, F.-S. Zhang, G. Zhao, C. Lin, and Y.-C. Jiao, "A loaded wideband linearly tapered slot antenna with broad beamwidth," *IEEE Antennas Wireless Propag. Lett.*, vol. 10, pp. 79–82, Jan. 2011.
[21] X. Chen, P.-Y. Qin, Y. J. Guo, and G. Fu, "Low-profile and wide-beamwidth dual-polarized distributed microstrip antenna," *IEEE Access*, vol. 5, pp. 2272–2280, Jan. 2017.
[22] J. Kornprobst, K. Wang, G. Hamberger, and T. F. Eibert, "A mm-wave patch antenna with broad bandwidth and a wide angular range," *IEEE Trans. Antennas Propag.*, vol. 65, no. 8, pp. 4293–4298, Aug. 2017.
[23] C.-M. Liu, S. Xiao, Z. Zhang, and J. Feng, "Low profile SIW slot antenna with wide beam-width radiation pattern," *Electron. Lett.*, vol. 54, no. 3, pp. 116–118, Feb. 2018.
[24] B. Feng, K. L. Chung, J. Lai, and Q. Zeng, "A conformal magneto-electric dipole antenna with wide H-plane and band-notch radiation characteristics for Sub-6-GHz 5G base-station," *IEEE Access*, vol. 7, pp. 17469–17479, 2019.
[25] B. Feng, L. Li, K. L. Chung, and Y. Li, "Wideband widebeam dual circularly-polarized magnetoelectric dipole Antenna/Array with meta-columns loading for 5G and beyond," *IEEE Trans. Antennas Propag.*, early access, Jul. 16, 2020, doi: 10.1109/TAP.2020.3008632.
[26] Z.-K. Pan, W.-X. Lin, and Q.-X. Chu, "Compact wide-beam circularly-polarized microstrip antenna with a parasitic ring for CNSS application," *IEEE Trans. Antennas Propag.*, vol. 62, no. 5, pp. 2847–2850, May 2014.
[27] C.-A. Yu, E. S. Li, H. Jin, Y. Cao, G.-R. Su, W. Che, and K.-S. Chin, "24 GHz horizontally polarized automotive antenna arrays with wide fan beam and high gain," *IEEE Trans. Antennas Propag.*, vol. 67, no. 2, pp. 892–904, Feb. 2019.
[28] C.-A. Yu, K.-S. Chin, and R. Lu, "24-GHz wide-beam patch antenna array laterally loaded with parasitic strips," in *Proc. Cross Strait Quad-Regional Radio Sci. Wireless Technol. Conf. (CSQRWC)*, Taiyuan, China Jul. 2019, pp. 1–3.
[29] W. L. Stutzman and G. A. Thiele, *Antenna Theory and Design*, 3rd ed. New York, NY, USA: Wiley, 2012.
[30] T. Mikulasek and J. Lacik, "Two feeding methods based on substrate integrated waveguide for microstrip patch antennas," *IET Microw., Antennas Propag.*, vol. 9, no. 5, pp. 423–430, Apr. 2015.

[31] M. Henry, C. E. Free, B. S. Izqueirdo, J. Batchelor, and P. Young, "Millimeter wave substrate integrated waveguide antennas: Design and fabrication analysis," *IEEE Trans. Adv. Packag.*, vol. 32, no. 1, pp. 93–100, Feb. 2009.
[32] J. Mayer, M. Martina, T. Gottwald, and T. Zwick, "PCB laminates for automotive radar antenna modules under different environmental conditions," *IEEE Trans. Antennas Propag.*, vol. 67, no. 9, pp. 6051–6058, Sep. 2019.
[33] N. A. Aboserwal, C. A. Balanis, and C. R. Birtcher, "Impact of coated ground-plane edge diffractions on amplitude patterns of circular apertures," *IEEE Antennas Wireless Propag. Lett.*, vol. 14, pp. 221–224, Feb. 2015.

GUAN-REN SU was born in Tainan City, Taiwan, in 1994. He received the B.S. degree in electrical engineering from the National Kaohsiung University of Science and Technology, Kaohsiung City, Taiwan, in 2016, and the M.S. degree in electrical engineering from the National Taipei University of Technology, Taipei City, Taiwan, in 2020.

His research interests include microwave circuit and antennas.

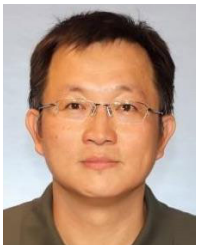

ERIC S. LI received the B.S. degree from Tamkang University, New Taipei City, Taiwan, in 1986, the M.S. degree in electrical engineering from the State University of New York, Stony Brook, NY, USA, in 1987, and the Ph.D. degree in electrical engineering from the University of Michigan, Ann Arbor, MI, USA, in 1998.

From 1988 to 1992 and from 1998 to 1999, he was in wireless industries as a Microwave Engineer participating in the designs of microwave circuits and antennas. From 1999 to 2006, he was a Faculty Member with the Department of Electrical Engineering, National Chi Nan University, Taiwan. Since 2006, he has been with the Department of Electronic Engineering, National Taipei University of Technology, Taiwan, where he is currently a Professor. His research interests include high-frequency circuits, high-frequency calibration and measurement techniques, microwave and millimeter-wave polarimetric radar systems, and electromagnetic scattering.

TING-WEI KUO was born in Taipei City, Taiwan. He received the B.S. degree in electronic engineering from Chang Gung University, Taoyuan City, Taiwan, in 2019, where he is currently pursuing the M.S. degree in electronic engineering.

His research interests include microwave circuit and automotive radar antennas.

HUAYAN JIN (Member, IEEE) was born in Hangzhou, Zhejiang, China, in 1989. She received the B.S. degree in electronic engineering and the Ph.D. degree in electromagnetic field and microwave technology from the Nanjing University of Science and Technology (NUST), Nanjing, China, in 2011 and 2017, respectively.

From August 2012 to January 2013, from May 2013 to October 2013, and from April 2014 to October 2014, she was an Exchange Student with Chang Gung University, Taoyuan City, Taiwan. She is currently a Lecturer with the School of Electronics and Information, Hangzhou Dianzi University, Hangzhou. Her research interests include millimeter-wave antennas, differential-fed antennas, and filtering antennas. She also serves as a Reviewer for the *IET Microwaves*, *Antennas & Propagation*, *IET Electronics Letters*, IEEE Access, and *International Journal of RF and Microwave Computer-Aided Engineering*.

YI-CHYUN CHIANG (Senior Member, IEEE) received the B.S. degree in marine technology from National Chiao-Tung University, Hsinchu, Taiwan, in 1982, and the M.S. and Ph.D. degrees in electronic engineering from Chiao-Tung University, Hsinchu, in 1987 and 1992, respectively. He is currently a Professor with the Department of Electronic Engineering, Chang Gung University, Taoyuan City, Taiwan, R.O.C. His research interests include the development of new design methods in realization of high performance microwave couplers and filters with very compact sizes and the development of microwave active circuits constructed with modern IC technologies. He is listed in 2006 Marquis who's who in World and IBC Top 100 Engineers in 2008.

KUO-SHENG CHIN (Senior Member, IEEE) received the B.S. degree in electrical engineering from the Chung Cheng Institute of Technology, Taoyuan City, Taiwan, in 1986, the M.S.E.E. degree from Syracuse University, Syracuse, NY, USA, in 1993, and the Ph.D. degree in communication engineering from National Chiao Tung University, Hsinchu, Taiwan, in 2005.

From 1986 to 2005, he was with the Chung Shan Institute of Science and Technology, Taoyuan City, as a Research Assistant, becoming an Assistant Scientist, and then an Associate Scientist. He joined Chang Gung University, Taoyuan City, as a Faculty Member, in 2006, where he is currently a Professor with the Department of Electronic Engineering. He has supervised a student team to win first place in the 2009 National Electromagnetism Application Innovation Competition, Taiwan. His current research interests include microwave and millimeter-wave couplers, filters, duplexers, low-temperature cofired ceramic circuits, automotive radar antennas, frequency-selective surfaces, filtering antennas, radomes, and electromagnetic pulse research. He was one of the recipients of the Best Paper Award of the International Conference on Electromagnetic Near Field Characterization and Imaging in 2009, the Honorable Paper Award of the International High Speed Intelligent Communication Forum in 2010, the Best Student Paper Award of the International Symposium on Next-Generation Electronics in 2014, the Best Paper Award of the Taiwan Precision Engineering Workshop in 2016, and the Best Student Paper Award of 2018 The 8th International Symposium on InfoComm & Mechatronics Technology in Bio-Medical & Healthcare Application. He received the Outstanding Teaching Award from Chang Gung University in 2014. He has served as an Associate Editor for *Microwave and Optical Technology Letters* from 2019 to 2020.